


RESEARCH ARTICLE | FEBRUARY 16 2023

Quarter-wavelength E||H Beltrami cavity resonators

Ryo Mochizuki  ; Naoki Shinohara ; Atsushi Sanada



AIP Advances 13, 025158 (2023)

<https://doi.org/10.1063/5.0138601>

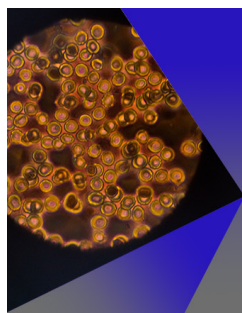


CrossMark

Articles You May Be Interested In

Zero Poynting vector E || H Beltrami field cylindrical cavity resonators

AIP Advances (July 2022)



AIP Advances

Special Topic: Medical Applications of Nanoscience and Nanotechnology

Submit Today!



Quarter-wavelength E||H Beltrami cavity resonators

Cite as: AIP Advances 13, 025158 (2023); doi: 10.1063/5.0138601

Submitted: 13 December 2022 • Accepted: 30 January 2023 •

Published Online: 16 February 2023



Ryo Mochizuki,^{1,a)} Naoki Shinohara,¹ and Atsushi Sanada²

AFFILIATIONS

¹Research Institute for Sustainable Humanosphere, Kyoto University, Uji, Kyoto, 611-0011, Japan

²Graduate School of Engineering Science, Osaka University, Toyonaka, Osaka, 560-8531, Japan

^{a)}Author to whom correspondence should be addressed: ryo_mochizuki@rish.kyoto-u.ac.jp

ABSTRACT

In this paper, we present the design and implementation methods of quarter-wavelength resonators accommodating Beltrami standing waves with parallel electric and magnetic (E||H) fields. The resonator is bounded by the quarter-wavelength longitudinal electromagnetic conductor (LEMC), the circumferential electromagnetic conductor (CEMC), and the radial electromagnetic conductor (REMC). The LEMC, CEMC, and REMC boundaries are artificially implemented by the circumferentially aligned corrugation, concentrically aligned circular fins, and axisymmetrically aligned radial fins, respectively. The coupling control methods by introducing slots in the CEMC and REMC with the external TM₀₁ and TE₀₁ circular waveguides are presented. We design the quarter-wavelength resonators with the implemented LEMC, CEMC, and REMC boundaries with controlled external couplings and numerically demonstrate their E||H properties, which confirms the validity of the proposed design method.

© 2023 Author(s). All article content, except where otherwise noted, is licensed under a Creative Commons Attribution (CC BY) license (<http://creativecommons.org/licenses/by/4.0/>). <https://doi.org/10.1063/5.0138601>

I. INTRODUCTION

The Beltrami cylindrical cavity resonator whose resonant mode has a unique property of the spatially and temporally parallel electric and magnetic fields has been proposed.¹ The fields in the Beltrami cylindrical cavity resonator are represented as

$$\mathbf{E} = e^{-i\omega t} E_0 \left[\frac{\beta}{k_c} J_1(k_c \rho) \sin(\beta z) \mathbf{e}_\rho \pm \frac{k_0}{k_c} J_1(k_c \rho) \cos(\beta z) \mathbf{e}_\varphi + J_0(k_c \rho) \cos(\beta z) \mathbf{e}_z \right], \quad (1)$$

$$\mathbf{H} = -ie^{-i\omega t} H_0 \left[\frac{\beta}{k_c} J_1(k_c \rho) \sin(\beta z) \mathbf{e}_\rho \pm \frac{k_0}{k_c} J_1(k_c \rho) \cos(\beta z) \mathbf{e}_\varphi + J_0(k_c \rho) \cos(\beta z) \mathbf{e}_z \right], \quad (2)$$

where a is the radius of the cavity, k_0 is the wavenumber number in vacuum, k_c is the cut-off wavenumber, β is the phase constant, and the relationship $\beta = \sqrt{k_0^2 - k_c^2}$ holds. The resonant fields of Eqs. (1) and (2) are a superposition of the TM₀₁ and its electromagnetically dual TE standing waves with the same amplitudes and

$\pm\pi/2$ spatial phase difference¹ and are spatially and temporally parallel with each other.²⁻¹³ The existence of the resonant modes in the cavity resonator perfectly isolated from the external circuits has been numerically confirmed. In order to excite the resonator in practical use, excitation schemes with (a) compatibility with the Beltrami fields and (b) individual controllability of TM and TE resonances are indispensable; however, the physical implementation and design methods of the excitation scheme have not been proposed yet.

In this paper, we propose an implementation method for the Beltrami resonators with individual TM and TE coupling control functionalities. According to Eqs. (1) and (2), the electric and magnetic fields in the transverse plane have only circumferential components E_φ and H_φ at $\beta z = 0$, whereas they have only radial components E_ρ and H_ρ at $\beta z = \pi/2$. Exploiting this fact, we propose an excitation method by introducing a quarter-wavelength resonator with complementary artificial boundaries that are compatible with the Beltrami fields with individual controllability. In the following, the implementation methods of the quarter-wavelength resonator and the artificial boundaries are presented, and the E||H Beltrami field generation is demonstrated.

II. BELTRAMI RESONATOR WITH COUPLING CONTROL FUNCTIONALITY

A. Quarter-wavelength Beltrami resonators

Figure 1 shows the proposed Beltrami resonator with independent TM and TE coupling control functionalities. The resonator is a LEMC waveguide terminated by singular boundary conditions, i.e., (a) a circumferential electromagnetic conductor (CEMC) enforcing $E_\varphi = 0$ and $H_\rho = 0$ (presented in the previous study¹) and (b) a radial electromagnetic conductor (REMC) enforcing $E_\rho = 0$ and $H_\varphi = 0$ (presented in this paper). The CEMC boundary operates as open- and short-circuited boundaries for TM and TE modes, respectively, whereas the REMC boundary operates as short- and open-circuited boundaries for TM and TE modes, respectively. This leads to the quarter-wavelength Beltrami resonant field.

The CEMC and REMC boundary conditions can be artificially implemented with the coupling control functionality of conventional TM_{01} and TE_{01} circular waveguides, respectively. It is noted that the coupling coefficient designs to generate the Beltrami fields are not trivial since the TM and TE field distributions differ and their unloaded Qs are not identical.

Figure 2 shows the implemented Beltrami resonator with the quarter-wavelength LEMC waveguide, the CEMC component, and the REMC component. The LEMC waveguide is implemented by circumferential corrugation.¹ The design methods of the CEMC and REMC components are presented in the following.

B. Circumferential electromagnetic conductor with coupling control functionality

The CEMC boundary is implemented by concentrically aligned circular fins with depth d_{CEMC} and thickness t_{CEMC} shown in Fig. 2(c). The circular fin depth d_{CEMC} is supposed to be $\lambda_0/4$ so that the incident TM and TE modes can be reflected with the reflection coefficients of 1 and -1 , respectively. This results in $E_\varphi = 0$ and $H_\rho = 0$ on the surface.

This component of Fig. 2(c) has coupling control functionality with an external TM_{01} circular waveguide with the narrow arc slots axially aligned at the bottom. The coupling coefficient, κ_{TM} , can be tuned by changing the slot width w_s^{CEMC} , the slot thickness t_s^{CEMC} , the arc radius ρ_s^{CEMC} , the arc angle φ_s^{CEMC} , and the number of the slots N_s^{CEMC} .

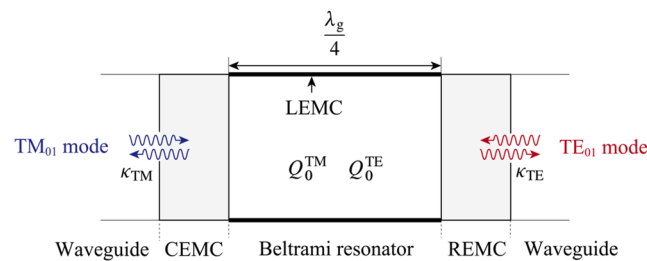


FIG. 1. Quarter-wavelength E||H Beltrami resonator composed of the LEMC waveguide and the CEMC/REMC components. The resonator is coupled to TM and TE feeding waveguides via small apertures in the CEMC and REMC components, respectively. κ_{TM} and κ_{TE} are the coupling coefficients from the external TM_{01} and TE_{01} waveguides, respectively.

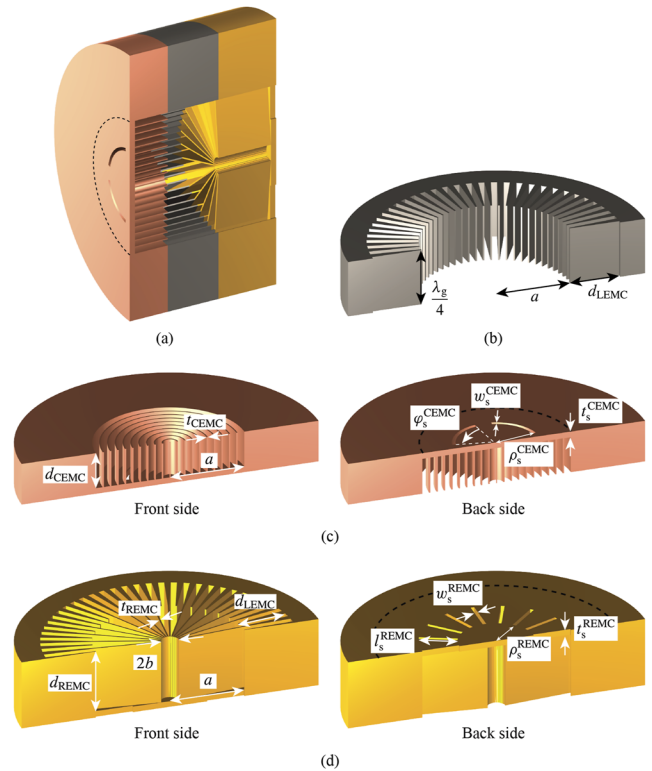


FIG. 2. Quarter-wavelength Beltrami resonator implementation cut on the plane, including the axis. (Only a half portion is shown.) (a) The general view. (b) The LEMC waveguide with the length L . a is the inner radius and d_{LEMC} is the corrugation depth. (c) The CEMC boundary implementation. d_{CEMC} is the fin depth, t_{CEMC} is the fin thickness, w_s^{CEMC} is the slot width, t_s^{CEMC} is the slot thickness, ρ_s^{CEMC} is the arc radius, and φ_s^{CEMC} is the arc angle. (d) The REMC boundary implementation. b is the center hole radius, d_{REMC} is the fin depth, t_{REMC} is the fin thickness, w_s^{REMC} is the slot width, t_s^{REMC} is the slot thickness, ρ_s^{REMC} is the arc radius, and φ_s^{REMC} is the arc angle. The dashed half-circles in (a), (c), and (d) represent the periphery of the feeding circular waveguides.

C. Radial electromagnetic conductor with coupling control functionality

The REMC boundary is implemented by radially aligned fins in a short-circuited LEMC waveguide, as shown in Fig. 2(d). The thickness of the fin t_{REMC} is supposed to be sufficiently smaller than the wavelength so that the incoming TE wave with the orthogonal electric field pattern toward the radial fins penetrates the REMC boundary on the surface and is reflected at the bottom. The depth of the fin d_{REMC} is chosen to be $\pi/(2\beta)$, where β is the phase constant of the TE wave inside the REMC, which is identical to that of the TE wave in the resonator. Therefore, the incoming TE wave is reflected with the reflection coefficient of e^{i0} at the REMC surface, whereas the incoming TM wave is reflected with the reflection coefficient of $e^{i\pi}$ at the REMC surface due to the radial fins. This leads to $E_\rho = 0$ and $H_\varphi = 0$ on the surface. Incidentally, since the electric field of the incoming TE wave on the axis is zero, the conductor in the region $0 \leq \rho \leq b$ ($b \ll a$) is removed for fabrication convenience.

This device of Fig. 2(d) also has the coupling control functionality with an external TE₀₁ circular waveguide with the narrow radial slots axisymmetrically aligned at the bottom. The coupling coefficient, κ_{TE} , can be determined by choosing the slot width w_s^{REMC} , the slot length l_s^{REMC} , the radial position ρ_s^{REMC} , the slot thickness t_s^{REMC} , and the number of the slots N_s^{REMC} .

III. DESIGN METHOD

An E||H Beltrami field is theoretically obtained as a superposition of the TM and TE modes with the same amplitude, i.e., with identical TM and TE stored energies in the resonator. However, in reality, it is not trivial to store the identical TM and TE mode energies in the proposed resonator structure since the effective LEMC radii differ for the TM and TE modes, and the TM and TE fields distribute differently in the CEMC and REMC components as well. Here, we theoretically derive the E||H resonant condition based on circuit theory.

A. Equivalent circuit model for the Beltrami resonator

We introduce two individual equivalent circuits for the orthogonal TM and TE modes, each with a series RLC resonator coupled to an external feeding line shown in Fig. 3. Let us refer to the TM and TE feeding lines as Ports 1 and 2, respectively. In the TM resonator of Fig. 3(a), the resonator end on the Port 2 side is short-circuited since the TM mode is perfectly reflected at the surface of the REMC boundary on the Port 2 side with a reflection coefficient of -1 . The resonator end on the Port 1 side is coupled to the external TM feeding line via an ideal transformer with a turns ratio $1 : n_{TM}$. In contrast, for the TE resonator of Fig. 3(b), the resonator end in the Port 1 side is short-circuited since the TE mode is perfectly reflected at the surface of the CEMC boundary in the Port 1 side with the reflection coefficient of -1 . The resonator end in the Port 2 is coupled to the external TE feeding line via an ideal transformer with a turns ratio $1 : n_{TE}$ as well. It is noted that the resistance in each

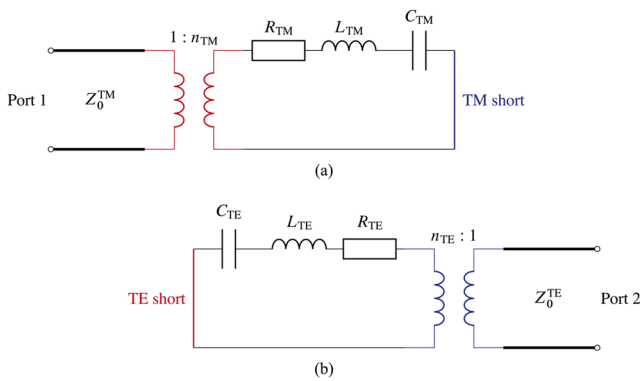


FIG. 3. Equivalent circuits for (a) the TM resonance and for (b) the TE resonance. The TM equivalent circuit is coupled to the feeding line with the characteristic impedance Z_0^{TM} via the ideal transformer with a turns ratio of $1 : n_{\text{TM}}$. The TE equivalent circuit is coupled to the feeding line with the characteristic impedance Z_0^{TE} via the ideal transformer with a turns ratio of $1 : n_{\text{TE}}$. Ports 1 and 2 are assigned on the sides of the TM and TE feeding lines, respectively.

circuit includes all the losses in the resonator and the CEMC and REMC components.

B. E||H condition

In order to obtain the E||H condition, let us first calculate the stored energies in the TM and TE resonators. According to equivalent circuits in Fig. 3, the unloaded Qs for the TM and TE resonators are readily obtained by

$$Q_0^{\text{TM}} = \frac{\omega_0^{\text{TM}} L_{\text{TM}}}{R_{\text{TM}}} = \frac{1}{\omega_0^{\text{TM}} C_{\text{TM}} R_{\text{TM}}}, \quad (3)$$

$$Q_0^{\text{TE}} = \frac{\omega_0^{\text{TE}} L_{\text{TE}}}{R_{\text{TE}}} = \frac{1}{\omega_0^{\text{TE}} C_{\text{TE}} R_{\text{TE}}}, \quad (4)$$

where L_{TM} and C_{TM} are the inductance and capacitance in the TM resonator, respectively, and L_{TE} and C_{TE} are the inductance and capacitance in the TE resonator, respectively, and ω_0^{TM} and ω_0^{TE} are the resonant angular frequencies of the TM and TE resonators, respectively. To realize the E||H fields, the TM and TE resonant frequencies ω_0^{TM} and ω_0^{TE} have to be identical, i.e.,

$$\omega_0^{\text{TM}} = \omega_0^{\text{TE}} = \frac{1}{\sqrt{L_{\text{TM}} C_{\text{TM}}}} = \frac{1}{\sqrt{L_{\text{TE}} C_{\text{TE}}}} \equiv \omega_0. \quad (5)$$

Under this condition, the TM and TE stored energies at the resonance, U_{TM} and U_{TE} , are given by

$$U_{\text{TM}} = \frac{Q_0^{\text{TM}} P_{\text{in}}^{\text{TM}}}{\omega_0} = \frac{4Q_0^{\text{TM}} \kappa_{\text{TM}}}{\omega_0 (1 + \kappa_{\text{TM}})^2} P_1, \quad (6)$$

$$U_{\text{TE}} = \frac{Q_0^{\text{TE}} P_{\text{in}}^{\text{TE}}}{\omega_0} = \frac{4Q_0^{\text{TE}} \kappa_{\text{TE}}}{\omega_0 (1 + \kappa_{\text{TE}})^2} P_2, \quad (7)$$

where P_1 and P_2 are the available powers of the sources of Port 1 and Port 2, respectively, and $P_{\text{in}}^{\text{TM}}$ and $P_{\text{in}}^{\text{TE}}$ are the powers flowed into the TM and TE resonators, respectively, and κ_{TM} and κ_{TE} are coupling coefficients of the TM and TE external circuits given by

$$\kappa_{\text{TM}} = \frac{n_{\text{TM}}^2 Z_0^{\text{TM}}}{R_{\text{TM}}}, \quad (8)$$

$$\kappa_{\text{TE}} = \frac{n_{\text{TE}}^2 Z_0^{\text{TE}}}{R_{\text{TE}}}. \quad (9)$$

Incidentally, $P_{\text{in}}^{\text{TM}}$ and $P_{\text{in}}^{\text{TE}}$ are written with the reflection coefficients $|S_{11}(\omega_0)|$ and $|S_{22}(\omega_0)|$ as

$$P_{\text{in}}^{\text{TM}} = (1 - |S_{11}(\omega_0)|^2) P_1, \quad (10)$$

$$P_{\text{in}}^{\text{TE}} = (1 - |S_{22}(\omega_0)|^2) P_2. \quad (11)$$

Therefore, according to Eqs. (6) and (7) with $P_1 = P_2$, the ratio of U_{TM} and U_{TE} is given by

$$\frac{U_{\text{TE}}}{U_{\text{TM}}} = \frac{\kappa_{\text{TE}} (1 + \kappa_{\text{TM}})^2}{\kappa_{\text{TM}} (1 + \kappa_{\text{TE}})^2} \frac{Q_0^{\text{TE}}}{Q_0^{\text{TM}}}. \quad (12)$$

In reality, the stored energies of Eqs. (6) and (7) are distributed not only inside the resonator but also in the CEMC and REMC components. In addition, the stored energies inside the TM and TE resonators differ due to the artificial LEMC boundary implementation with the corrugation. As for the TM resonator, the energy is stored in the resonator and the CEMC component. The energy ratio in the resonator is expressed by $U_{TM}/(1 + \alpha_{TM})$, where α_{TM} is the ratio between the energy in the resonator and that in the CEMC component [see Fig. 4(a)]. As for the TE resonator, the energy is stored inside the resonator, the REMC component, and the LEMC corrugation. The energy ratio in the resonator is expressed by $U_{TE}/(2(1 + \alpha_{TE}))$, where α_{TE} is the ratio between the energy in the resonator and that in the LEMC corrugation considering the fact that the energy in the REMC component is identical to the total energy in the resonator and the LEMC corrugation [see Fig. 4(b)].

The $\mathbf{E}\parallel\mathbf{H}$ Beltrami field occurs when the TM and TE energies inside the resonator except for the LEMC corrugation agree with each other. Consequently, we obtain

$$\frac{U_{TM}}{1 + \alpha_{TM}} = \frac{U_{TE}}{2(1 + \alpha_{TE})}. \tag{13}$$

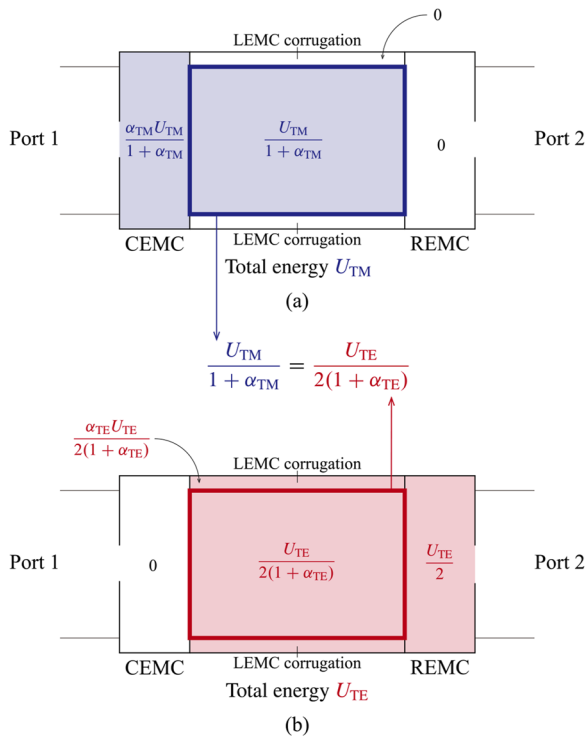


FIG. 4. The energy distributions of (a) the TM mode and (b) the TE mode. The total energies in the TM and TE mode resonances are denoted as U_{TM} and U_{TE} , respectively. The TM stored energy in the resonator region enclosed by the blue line is $U_{TM}/(1 + \alpha_{TM})$. The TE stored energy in the resonator region enclosed by the red line is $U_{TE}/(2(1 + \alpha_{TE}))$. The $\mathbf{E}\parallel\mathbf{H}$ Beltrami resonance occurs under the condition $U_{TM}/(1 + \alpha_{TM}) = U_{TE}/(2(1 + \alpha_{TE}))$.

Note that the stored energy ratios α_{TM} and α_{TE} are theoretically obtained from the mode matchings at the CEMC surface and the LEMC corrugation surface, respectively, as

$$\alpha_{TM} = \frac{a^2 \beta^3 \lambda_0}{2\pi(a^2 \beta^2 + p_{01}^2)} \tag{14}$$

$$\alpha_{TE} = \frac{(1 - D_{cor})\pi}{2p_{01}}. \tag{15}$$

See Appendix. By applying Eqs. (14) and (15) into Eq. (13), U_{TE}/U_{TM} is determined from the resonator radius a and the LEMC corrugation duty D_{cor} as

$$\frac{U_{TE}}{U_{TM}} = \frac{2 + (1 - D_{cor})\pi/p_{01}}{1 + (1 - p_{01}^2 \lambda_0^2 / (4a^2 \pi^2))^{\frac{1}{2}}} \equiv \frac{U_{TE}^*}{U_{TM}^*}, \tag{16}$$

where λ_0 is the wavelength in free space and p_{01} is the first zero of zeroth first kind Bessel function J_0 . Therefore, the $\mathbf{E}\parallel\mathbf{H}$ condition for κ_{TM} and κ_{TE} is obtained by applying Eq. (16) into Eq. (12) as

$$\frac{\kappa_{TE}}{\kappa_{TM}} \frac{(1 + \kappa_{TM})^2}{(1 + \kappa_{TE})^2} = \frac{U_{TE}^* Q_0^{TM}}{U_{TM}^* Q_0^{TE}}. \tag{17}$$

Note that any combination of κ_{TM} and κ_{TE} satisfying Eq. (17) gives an $\mathbf{E}\parallel\mathbf{H}$ field. Figure 5 depicts the relationship between κ_{TM} and κ_{TE} of Eq. (17) for specific $U_{TE}^* Q_0^{TM} / (U_{TM}^* Q_0^{TE})$ values of 0.125, 0.25, 0.5, 1, 2, 4, and 8. Note that the value of $U_{TE}^* Q_0^{TM} / (U_{TM}^* Q_0^{TE})$ is determined directly from the resonator structure and material. It is also noted that the relationship between κ_{TM} and κ_{TE} sufficiently smaller than unity, whereas the relationship deviates from a linear one depending on the $U_{TE}^* Q_0^{TM} / (U_{TM}^* Q_0^{TE})$ value.

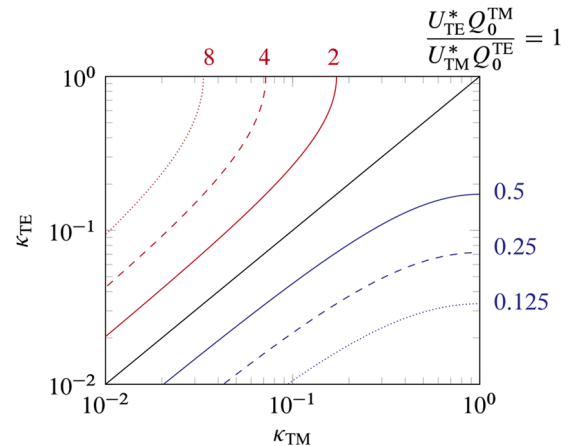


FIG. 5. The $\mathbf{E}\parallel\mathbf{H}$ resonant condition for the TM and TE coupling coefficients κ_{TM} and κ_{TE} for the specific $U_{TE}^* Q_0^{TM} / (U_{TM}^* Q_0^{TE})$ values of 0.125 (blue dotted line), 0.25 (blue dashed line), 0.5 (blue solid line), 1 (black solid line), 2 (red solid line), 4 (red dashed line), and 8 (red dotted line).

IV. NUMERICAL SIMULATIONS

A. Resonator design

We first determine the structure of a Beltrami resonator composed of the LEMC waveguide and CEMC/REMC components without coupling slots. We determine the resonant frequency to be 2.38 GHz and the lateral LEMC boundary to be implemented with 64 ϕ -segments of corrugation with the duty ratio $D_{\text{cor}} = 0.2$ considering realistic implementations. Then, by using a commercial finite element method based simulator, the High Frequency Structure Simulator (HFSS), we numerically obtain the effective LEMC radius a considering the fringing effect as 62.5 mm with a corrugation depth of 41.64 mm so that the TM and TE cut-off frequencies coincide with each other.¹ In the simulation, we use the conductivity of the resonator material as 5.8×10^8 S/m. The resonator length L is theoretically obtained from a as 48.57 mm accordingly. As for the CEMC component, let the CEMC be composed of ten equally spaced concentric fins with the fin thickness $t_{\text{CEMC}} = 1$ mm, as shown in Fig. 2(c). The fin depth d_{CEMC} is numerically determined as 31.16 mm by taking into account the fringing effect at the resonant frequency of 2.38 GHz. As for the REMC component, let the REMC be composed of 32 radial fins with fin thickness $t_{\text{REMC}} = 1.23$ mm with the center hole radius $b = 7.5$ mm, as shown in Fig. 2(d). The fin depth d_{REMC} is numerically determined as 50.75 mm by taking into account the fringing effect at the resonant frequency of 2.38 GHz.

B. External coupling designs for E||H realizations

Now, we realize the E||H resonance by determining the external coupling structures. According to eigenmode simulations by HFSS, the TM and TE unloaded Qs of the designed resonator are calculated as $Q_0^{\text{TM}} = 5.78 \times 10^3$ and $Q_0^{\text{TE}} = 3.92 \times 10^3$, respectively. On the other hand, from Eq. (16), the theoretical TM and TE stored energy ratio is

$$\frac{U_{\text{TE}}^*}{U_{\text{TM}}^*} = 2.42. \quad (18)$$

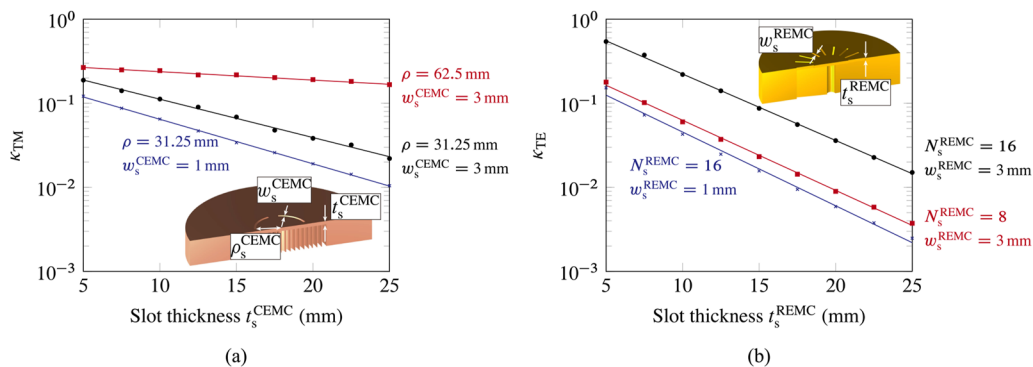


FIG. 6. The slot thickness dependences of (a) the TM coupling coefficient κ_{TM} and (b) the TE coupling coefficient κ_{TE} . The black, blue, and red lines in (a) correspond to the combinations of arc radius ρ_s^{CEMC} and the slot width w_s^{CEMC} of $(\rho_s^{\text{CEMC}}, w_s^{\text{CEMC}}) = (31.25 \text{ mm}, 3 \text{ mm})$, $(31.25 \text{ mm}, 1 \text{ mm})$, and $(62.5 \text{ mm}, 3 \text{ mm})$, respectively. The slot number N_s^{CEMC} is 4, and the arc angle ϕ_s^{CEMC} is $3\pi/8$. The black, blue, and red lines in (b) correspond to the combinations of the slot number N_s^{REMC} and the slot width w_s^{REMC} of $(N_s^{\text{REMC}}, w_s^{\text{REMC}}) = (16, 3 \text{ mm})$, $(16, 1 \text{ mm})$, and $(8, 3 \text{ mm})$, respectively. The radial slot position ρ_s^{REMC} is 31.25 mm, and the slot length l_s^{CEMC} is 31.25 mm. All the lines are fitted with least squares approximations.

Applying these Q_0^{TM} , Q_0^{TE} , and $U_{\text{TE}}^*/U_{\text{TM}}^*$ values to Eq. (17), the κ_{TM} and κ_{TE} have to satisfy

$$\frac{\kappa_{\text{TE}} (1 + \kappa_{\text{TM}})^2}{\kappa_{\text{TM}} (1 + \kappa_{\text{TE}})^2} = \frac{U_{\text{TE}}^* Q_0^{\text{TM}}}{U_{\text{TM}}^* Q_0^{\text{TE}}} = 3.50. \quad (19)$$

In order to determine the coupling slot structures, we numerically investigate the relationship between the slot dimension and the coupling coefficients. The coupling coefficients are calculated by the reflection coefficients $|S_{11}|$ and $|S_{22}|$ in Figs. 6(a) and 6(b) as

$$\kappa_{\text{TM}} = \frac{1 - |S_{11}|}{1 + |S_{11}|}, \quad (20)$$

$$\kappa_{\text{TE}} = \frac{1 - |S_{22}|}{1 + |S_{22}|}. \quad (21)$$

Figure 6(a) shows the slot thickness dependence of κ_{TM} for specific three slot dimensions. Here, the radius of the external feeding TM₀₁ circular waveguide is given as 62.5 mm so that its phase constant is identical to that of the resonant E||H Beltrami field inside the resonator. Note that the radius of the external feeding waveguide is arbitrary. The black and red lines are for arc radius $\rho_s^{\text{CEMC}} = 31.25$ mm and 62.5 mm, respectively. The other parameters are $w_s^{\text{CEMC}} = 3$ mm, $\phi_s^{\text{CEMC}} = 3\pi/8$, and $N_s^{\text{CEMC}} = 4$. It is seen from the figure that the coupling coefficient decreases with the slot thickness and the larger the arc radius ρ_s^{CEMC} , the larger the coupling coefficient κ_{TM} . The black and blue lines are for the slot width of $w_s^{\text{CEMC}} = 3$ and 1 mm, respectively. The other parameters are $\rho_s^{\text{CEMC}} = 31.25$ mm, $\phi_s^{\text{CEMC}} = 3\pi/8$, and $N_s^{\text{CEMC}} = 4$. It is seen from the figure that the coupling coefficient decreases with the slot thickness and the narrower the slot width w_s^{CEMC} , the smaller the coupling coefficient κ_{TM} . Figure 6(b) shows the slot thickness dependence of κ_{TE} for specific three slot dimensions. Here, the radius of the external feeding TE₀₁ circular waveguide is given as 99.58 mm so that its phase constant is identical to that of the resonant E||H Beltrami field inside the resonator. Note that the radius of the external feeding waveguide is arbitrary. The black and red lines are for the slot

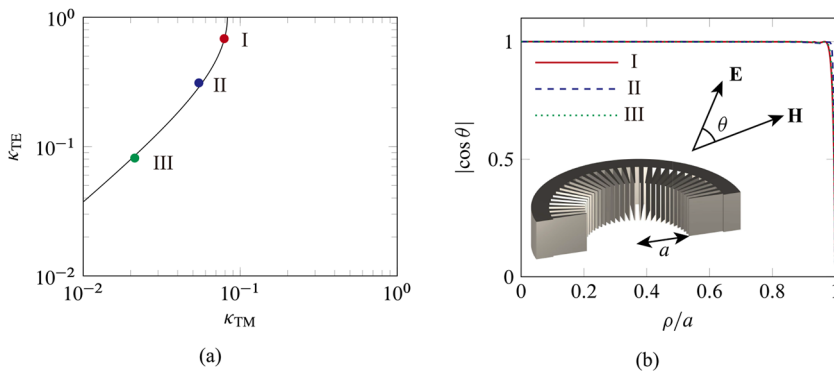


FIG. 7. The relation between κ_{TM} and κ_{TE} for $\mathbf{E}\parallel\mathbf{H}$ fields (a) and the ρ -dependence of $|\cos \theta|$ for the three κ_{TM} and κ_{TE} combinations (b). The red, blue, and green points in (a) correspond to $(\kappa_{TM}, \kappa_{TE}) = (7.90 \times 10^{-2}, 6.84 \times 10^{-1}), (5.45 \times 10^{-2}, 3.11 \times 10^{-1}),$ and $(2.13 \times 10^{-2}, 8.16 \times 10^{-2}),$ respectively.

number of $N_s^{REMC} = 16$ and 8, respectively. The other parameters are $w_s^{REMC} = 3$ mm, $l_s^{REMC} = 31.25$ mm, and $\rho_s^{REMC} = 31.25$ mm. It is seen from the figure that the coupling coefficient decreases with the slot thickness and the more the slot number N_s^{REMC} , the larger the coupling coefficient κ_{TE} . The black and blue lines are for the slot width of $w_s^{REMC} = 3$ and 1 mm, respectively. The other parameters are $N_s^{REMC} = 16, l_s^{REMC} = 31.25$ mm, and $\rho_s^{REMC} = 31.25$ mm. It is seen from the figure that the coupling coefficient decreases with the slot thickness and the narrower the slot width w_s^{REMC} , the smaller the coupling coefficient κ_{TE} .

The curve in Fig. 7(a) is the κ_{TM} and κ_{TE} relationship of Eq. (19) for the designed resonator. In order to examine the $\mathbf{E}\parallel\mathbf{H}$ resonance, we arbitrarily choose the three $(\kappa_{TM}, \kappa_{TE})$ points of $(7.90 \times 10^{-2}, 6.84 \times 10^{-1}), (5.45 \times 10^{-2}, 3.11 \times 10^{-1}),$ and $(2.13 \times 10^{-2}, 8.16 \times 10^{-2})$ on the curve, and the field distributions in the

three resonators corresponding to the points are numerically calculated. The TM and TE coupling slot dimensions at Port 1 and Port 2 are determined according to each set of coupling coefficients $(\kappa_{TM}, \kappa_{TE})$, respectively. The slot dimensions are summarized in Table I. Figure 7(b) shows the ρ -dependence of $|\cos \theta|$ on the transverse section $z = L/2$ for the three resonators, where θ is the angle between the \mathbf{E} and \mathbf{H} vectors. The value of $|\cos \theta|$ represents $|\mathbf{E} \cdot \mathbf{H}| / (|\mathbf{E}||\mathbf{H}|)$, and the \mathbf{E} and \mathbf{H} vectors are parallel or antiparallel with the value of unity, whereas the \mathbf{E} and \mathbf{H} vectors are orthogonal with the value of null. It is seen from Fig. 7(b) that the value of $|\cos \theta|$ is almost unity for each κ_{TM} and κ_{TE} combination except in the vicinity of the periphery ($\rho/a \sim 1$) due to the local field perturbations by the corrugation. Figure 8 shows an example of the time series snapshots of electromagnetic field distributions on the transverse section $z = L/2$ for the coupling coefficient combination

TABLE I. The TM and TE slot dimensions for the coupling coefficients κ_{TM} and κ_{TE} satisfying the $\mathbf{E}\parallel\mathbf{H}$ condition. The numbers of the TM and TE slots are 4 and 16, respectively. The TM slot dimensions $w_s^{CEMC}, t_s^{CEMC}, \rho_s^{CEMC},$ and φ_s^{CEMC} represent the slot width, the slot thickness, the arc radius, and the arc angle, respectively. The TE slot dimensions $w_s^{REMC}, l_s^{REMC}, \rho_s^{REMC},$ and t_s^{REMC} represent the slot width, the slot length, the radial position, and the slot thickness, respectively.

$(\kappa_{TM}, \kappa_{TE})$	w_s^{CEMC} (mm)	t_s^{CEMC} (mm)	ρ_s^{CEMC} (mm)	φ_s^{CEMC}	w_s^{REMC} (mm)	l_s^{REMC} (mm)	ρ_s^{REMC} (mm)	t_s^{REMC} (mm)
$(7.90 \times 10^{-2}, 6.84 \times 10^{-1})$	3	13	31.25	$3\pi/8$	3	31.25	31.25	2
$(5.45 \times 10^{-2}, 3.11 \times 10^{-1})$	3	17	31.25	$3\pi/8$	3	31.25	31.25	8.3
$(2.13 \times 10^{-2}, 8.16 \times 10^{-2})$	3	25	31.25	$3\pi/8$	3	31.25	31.25	15.3

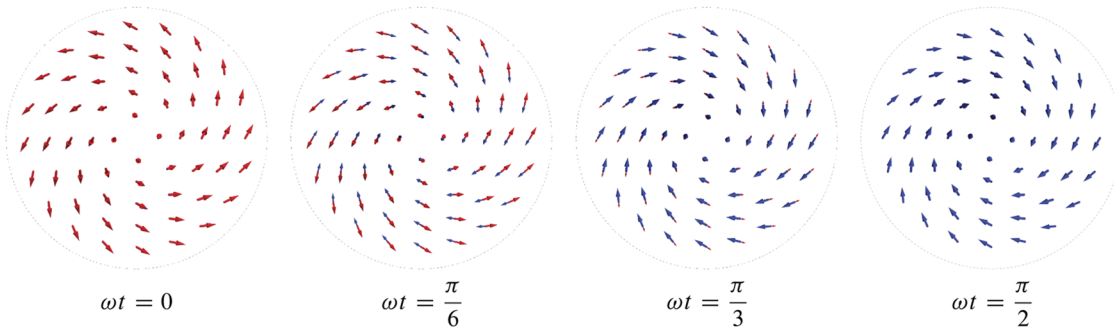


FIG. 8. The time-series snapshots of the electric and magnetic field distributions on the transverse section $z = L/2$ for the resonator with $(\kappa_{TM}, \kappa_{TE}) = (5.45 \times 10^{-2}, 3.11 \times 10^{-1})$. The red arrows represent the electric field vector, whereas the blue arrows represent the magnetic field vector.

$(\kappa_{TM}, \kappa_{TE}) = (7.90 \times 10^{-2}, 6.84 \times 10^{-1})$. It is seen from the figure that the electric and magnetic fields are parallel with each other both spatially and temporally. From these results, we can conclude that the $\mathbf{E} \parallel \mathbf{H}$ Beltrami resonance is realized by choosing coupling slot parameters so that the coupling coefficients satisfy Eq. (17), and the validity of the presented design method is confirmed.

V. CONCLUSIONS

In this paper, we have presented the design and realistic implementation methods of the quarter-wavelength $\mathbf{E} \parallel \mathbf{H}$ Beltrami cavity resonators using CEMC and REMC boundary components. Implementation methods of the CEMC and REMC boundaries with the TM and TE coupling control functionalities have been shown. We have theoretically derived the relation between the TM and TE coupling coefficients for the $\mathbf{E} \parallel \mathbf{H}$ condition based on circuit theory. We have numerically designed the resonator operating at 2.38 GHz based on the design theory and numerically demonstrated the $\mathbf{E} \parallel \mathbf{H}$ Beltrami field generations in the resonator.

ACKNOWLEDGMENTS

This work was supported by the JSPS KAKENHI Grant No. JP20J14118.

AUTHOR DECLARATIONS

Conflict of Interest

The authors have no conflicts to disclose.

Author Contributions

Ryo Mochizuki: Conceptualization (lead); Data curation (lead); Formal analysis (lead); Investigation (lead); Methodology (equal); Validation (equal); Visualization (equal); Writing – original draft (lead); Writing – review & editing (equal). **Naoki Shinohara:** Conceptualization (supporting); Funding acquisition (lead); Investigation (supporting); Methodology (supporting); Project administration (equal); Resources (lead); Supervision (equal); Validation (equal); Writing – review & editing (equal). **Atsushi Sanada:** Conceptualization (supporting); Data curation (supporting); Formal analysis (supporting); Investigation (supporting); Methodology (equal); Project administration (equal); Supervision (equal); Validation (equal); Visualization (equal); Writing – original draft (supporting); Writing – review & editing (equal).

DATA AVAILABILITY

The data that support the findings of this study are available within the article.

APPENDIX: CALCULATIONS OF α_{TM} AND α_{TE}

In the LEMC, the TM electromagnetic field is represented with orthogonal wave functions for the circular waveguide, $\mathbf{e}_m^{\text{LEMC}}(\rho, \varphi, z)$ ($m = 1, 2, \dots$) as

$$\mathbf{E}^{\text{LEMC}}(\rho, \varphi, z) = E_0(\beta k_c^{-1} J_1(k_c \rho) \sin \beta z \mathbf{e}_\rho + J_0(k_c \rho) \mathbf{e}_z \cos \beta z) + \sum_m \mathbf{e}_m^{\text{LEMC}}(\rho, \varphi, z), \quad (\text{A1})$$

with the origin at the REMC center. Assuming that the higher mode energies are sufficiently small and neglected, the stored energy in the resonator, $U_{\text{TM}}^{\text{in}}$, is given by integrating the square of Eq. (A1) in the entire resonator region as

$$U_{\text{TM}}^{\text{in}} = \frac{a^2 \pi J_1(p_{01})^2 (a^2 \beta^2 + \pi p_{01}^2) \epsilon_0 E_0^2}{16 \beta p_{01}^2}. \quad (\text{A2})$$

In the CEMC, the electric field in the CEMC component is represented by the coaxial waveguide modes as

$$\mathbf{E}_{\text{CEMC}}(\rho, \varphi, z) = \frac{V_n}{\ln(r_n^{\text{in}}/r_n^{\text{out}})r} \cos(k_0(z - \pi/(2\beta))) \mathbf{e}_r + \sum_m \mathbf{e}_m^{\text{CEMC}}(\rho, \varphi, z), \quad (\text{A3})$$

where V_n is the voltage between the n - and $(n + 1)$ -th fins with n counted from inside, r_n^{out} and r_n^{in} are the outer radius of n th fin and the inner radius of $(n + 1)$ th fin, respectively, and $\mathbf{e}_m^{\text{CEMC}}$'s represents higher order modes of the coaxial waveguide. Due to the field continuity at the boundary $z = \beta/(2\pi)$, the fundamental mode between the n - and $(n + 1)$ -th fins is rewritten with Eq. (A1) as

$$\begin{aligned} & \frac{V_n}{\ln(r_n^{\text{in}}/r_n^{\text{out}})r} \cos(k_0(z - \pi/(2\beta))) \mathbf{e}_r \\ &= E_0[\beta k_c^{-1} J_1(k_c \rho) \cos(k_0(z - \pi/(2\beta))) \mathbf{e}_\rho] \\ &+ \sum_m [\mathbf{e}_m^{\text{LEMC}}(\rho, \varphi, \beta/(2\pi)) \\ &- \mathbf{e}_m^{\text{CEMC}}(\rho, \varphi, \beta/(2\pi))] \cos(k_0(z - \pi/(2\beta))). \end{aligned} \quad (\text{A4})$$

Therefore, the field energy between the n - and $(n + 1)$ -th fins, u_n^{CEMC} , is calculated as

$$u_n^{\text{CEMC}} = \int_{\rho_n^{\text{in}}}^{\rho_n^{\text{out}}} \int_0^{2\pi} \int_{\beta/(2\pi)}^{\pi/(2\beta) + \pi/(2k_0)} \rho |E_0 \beta k_c^{-1} J_1(k_c \rho) \cos(k_0(z - \pi/(2\beta)))|^2 d\varphi dz, \quad (\text{A5})$$

where all the higher mode energies in the LEMC and CEMC components are assumed to be sufficiently small and neglected. Assuming that the CEMC fin thickness is infinitely small, the total CEMC energy, U^{CEMC} , is calculated as

$$U^{\text{CEMC}} = \sum_n u_n^{\text{CEMC}} = \frac{a^4 \beta^2 \lambda_0 J_1(p_{01})^2 \epsilon_0 E_0^2}{32 p_{01}^2}. \quad (\text{A6})$$

Therefore, the TM energy ratio α_{TM} is

$$\alpha_{\text{TM}} = \frac{U^{\text{CEMC}}}{U_{\text{TM}}^{\text{in}}} = \frac{a^2 \beta^3 \lambda_0}{2\pi(a^2 \beta^2 + p_{01}^2)}. \quad (\text{A7})$$

The electric field of the TE mode in the LEMC region can be represented by taking into account the field continuity at $\rho = a$ as

$$\mathbf{E} = \begin{cases} E_0 J_1(k_c \rho) \cos(\beta z) \mathbf{e}_\varphi & (0 \leq \rho \leq a), \\ E_0 J_1(k_c a) \cos(k_c(\rho - a)) \cos(\beta z) \mathbf{e}_\varphi & (a \leq \rho \leq a + d_{\text{LEMC}}). \end{cases} \quad (\text{A8})$$

The stored energy in the resonator region $0 \leq \rho \leq a$, $U_{\text{TE}}^{\text{in}}$, is given by integrating the square of Eq. (A8) in the entire resonator region as

$$U_{\text{TE}}^{\text{in}} = \frac{a^2 \pi^2 J_1(p_{01})^2 \epsilon_0 E_0^2}{8\beta}. \quad (\text{A9})$$

The stored energy inside the corrugation, $U_{\text{TE}}^{\text{cor}}$, is calculated with the corrugation duty D_{cor} from Eq. (A8) as

$$U_{\text{TE}}^{\text{cor}} = \frac{a^2 \pi^3 (1 - D_{\text{cor}}) J_1(p_{01})^2 \epsilon_0 E_0^2}{16\beta p_{01}}. \quad (\text{A10})$$

From Eqs. (A9) and (A10), the energy ratio α_{TE} is given as

$$\alpha_{\text{TE}} = \frac{U_{\text{TE}}^{\text{cor}}}{U_{\text{TE}}^{\text{in}}} = \frac{(1 - D_{\text{cor}})\pi}{2p_{01}}. \quad (\text{A11})$$

REFERENCES

- ¹R. Mochizuki, N. Shinohara, and A. Sanada, "Zero Poynting vector E||H Beltrami field cylindrical cavity resonators," *AIP Adv.* **12**, 075314 (2022).
- ²A. Lakhtakia, *Beltrami Fields in Chiral Media* (World Scientific, 1994).
- ³K. K. Lee, "Comments on "transverse electromagnetic waves with $\vec{E} \parallel \vec{B}$,"" *Phys. Rev. Lett.* **50**, 138 (1983).
- ⁴C. Chu, "Chu responds," *Phys. Rev. Lett.* **50**, 139 (1983).
- ⁵H. Zaghoul, K. Volk, and H. A. Buckmaster, "Comment on "transverse electromagnetic waves with $\vec{E} \parallel \vec{B}$,"" *Phys. Rev. Lett.* **58**, 423 (1987).
- ⁶C. Chu and T. Ohkawa, "Chu and Ohkawa respond," *Phys. Rev. Lett.* **58**, 424 (1987).
- ⁷A. Khare and T. Pradhan, "Transverse electromagnetic waves with finite energy, action, and $\int \vec{E} \cdot \vec{B} d^4x$," *Phys. Rev. Lett.* **49**, 1227–1228 (1982).
- ⁸F. C. Michel, "Transverse electromagnetic waves with nonzero $\vec{E} \cdot \vec{B}$," *Phys. Rev. Lett.* **52**, 1351 (1984).
- ⁹H. Zaghoul and H. A. Buckmaster, "Transverse electromagnetic standing waves with $\vec{E} \parallel \vec{B}$," *Am. J. Phys.* **56**, 801–806 (1988).
- ¹⁰K. Shimoda, T. Kawai, and K. Uehara, "Electromagnetic plane waves with parallel electric and magnetic fields E||H in free space," *Am. J. Phys.* **58**, 394–396 (1990).
- ¹¹K. Uehara, T. Kawai, and K. Shimoda, "Non-transverse electromagnetic waves with parallel electric and magnetic fields," *J. Phys. Soc. Jpn.* **58**, 3570–3575 (1989).
- ¹²T. Nishiyama, "General plane or spherical electromagnetic waves with electric and magnetic fields parallel to each other," *Wave Motion* **54**, 58–65 (2015).
- ¹³R. Mochizuki, N. Shinohara, and A. Sanada, "Time-harmonic electromagnetic fields with $\vec{E} \parallel \vec{B}$ represented by superposing two counter-propagating beltrami fields," *Prog. Electromagn. Res. M* **104**, 171–184 (2021).